Front dynamics in an oscillatory bistable Belousov-Zhabotinsky chemical reaction

Bradley Marts, Karl Martinez, and Anna L. Lin*
Center for Nonlinear and Complex Systems and Department of Physics, Duke University, Durham, North Carolina 27708, USA
(Received 30 April 2004; published 29 November 2004)

We observe breathing front dynamics which select three distinct types of bistable patterns in the 2:1 resonance regime of the periodically forced oscillatory Belousov-Zhabotinsky reaction. We measure the curvature-driven shrinking of a circular domain $R \sim t^{1/2}$ at forcing frequencies below a specific value, and show that the fast time scale front oscillations (breathing) drive this slow time scale shrinking. Above a specific frequency, we observe fronts of higher curvature grow instead of shrink and labyrinth patterns form. Just below the transition frequency is a relatively narrow range of frequencies where the curvature-driven coarsening is balanced by a competing front interaction, which leads to a pattern of localized structures. The length scale of the localized structure and labyrinth patterns is set by the front interactions.

DOI: 10.1103/PhysRevE.70.056223 PACS number(s): 82.40.Bj, 05.45.Xt, 05.65.+b, 05.45.−a

I. INTRODUCTION

Bistability, the property that a system has two equally likely solutions, is found in equilibrium systems such as copolymers [1] and metal-ion clusters [2]; and in nonequilibrium systems such as driven circuits [3], semiconductors [4], lasers [5], and some chemical reactions [6–8]. In extended systems, bistability can cause pattern formation, i.e., different spatial arrangements of the two stable states. While the resulting pattern in equilibrium systems can often be understood in terms of minimizing a free energy, nonequilibrium systems are not driven by this principle.

We investigate how the front dynamics select patterns in the forced nonequilibrium Belousov-Zhabotinsky (BZ) chemical reaction. We periodically force the light-sensitive BZ reaction, with spatially homogeneous pulses of light, over a range of frequencies that lock in the 2:1 resonance regime of the forcing. The chemical concentration oscillates exactly once for every two forcing cycles and there are two stable (π-shifted) oscillating states [8,9]. We examine the slow time scale pattern evolution, i.e., on a time scale much longer than the chemical oscillation period, of the forced BZ system at high forcing strengths.

The BZ chemical reaction has been widely used to investigate mechanisms of pattern formation in nonequilibrium reaction diffusion systems. Resonances of the quasi-2D oscillatory BZ reaction with a periodic external forcing have been studied previously [6–14]. The propagation of excitation waves has also been studied in the context of the BZ reaction [15,16]. These previous works have found that fronts of different curvature propagate into the unexcited state at different velocities; a positive curvature front propagates more slowly and a negative curvature front more quickly. This is captured by the well known eikonal equation [17–19]

$$V = V_0 - D\kappa, \tag{1}$$

where V is the velocity normal to the front, V_o is the velocity of a flat front, D is a diffusion coefficient, and κ is the front curvature.

We observe that the slow front dynamics of the patterns in the high forcing strength regime of 2:1 resonance select either a stationary flat front separating spatially uniform domains of π-shifted oscillations, localized structures, or labyrinth patterns [8,9] depending on parameter values (see Fig. 1).

The forced complex Ginzburg-Landau (FCGL) equation is a generic amplitude equation for oscillatory systems near a Hopf bifurcation. Our experimental observations for the rates of pattern evolution and the pattern wavelengths selected are in agreement with results from the FCGL equation [20]. Even though our BZ experiments are conducted far from the Hopf bifurcation, the FCGL has predicted many results observed in the forced BZ system [10,11,21].

These patterns and the transitions between them have also been found in a resonant optical system [5] and in the amplitude equations which describe it [22]. Our experiments test the theoretical predictions in a different type of system, a chemically reactive system, and demonstrate the generality of these coarsening mechanisms. Furthermore, we describe the mechanism of the pattern formation in terms of the small-amplitude, fast oscillations (breathing motion) of the front propagation direction.

The organization of the rest of this paper is as follows. The physical setup and data analysis methods are described in Sec. II. The experimental results showing curvature-driven shrinking are presented in Sec. III A. The observation of localized structures is discussed in Sec. III B and labyrinths are discussed in Sec. III C. We develop a physical explanation of these mechanisms based on the chemical reaction and the two-dimensional (2D) geometry in Sec. IV.

II. METHODS

A. Experimental setup

We use the same BZ reactor setup as in [8,9,14]. The reaction takes place in a thin porous Vycor glass membrane sandwiched between two chemical reservoirs. The glass membrane is 0.4 mm thick and 22 mm in diameter. Reagents diffuse homogeneously from the continuously stirred reservoirs into the glass through its two faces. The pattern wave-

*Electronic address: alin@phy.duke.edu

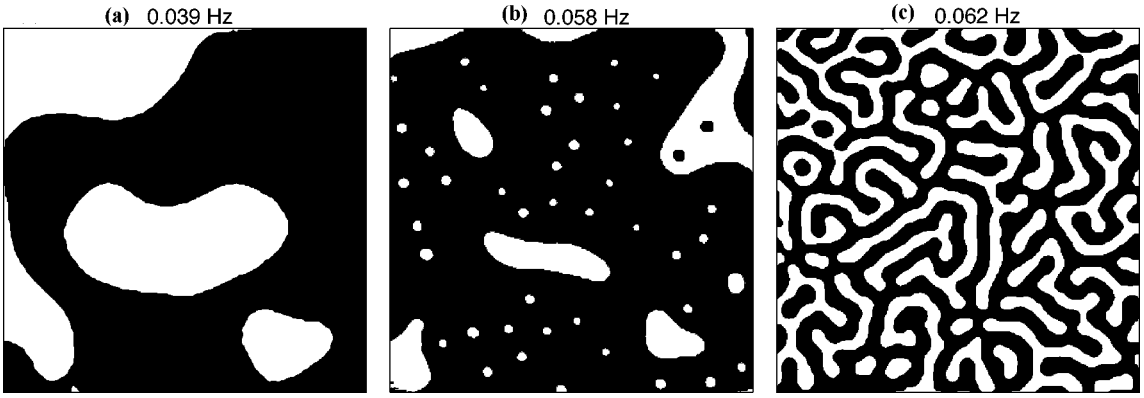

FIG. 1. Examples of (a) large domain, (b) localized structures, and (c) labyrinth patterns in the 2:1 resonant regime of the periodically forced BZ reaction. The forcing frequency, ω, increases from left to right. The pattern on the far left will eventually evolve into a single flat front. The small domains in (b) are stationary while larger domains continue to shrink. The labyrinth in (c) is stationary. Chemical conditions are given in Sec. II A. Image sizes are (a) 11.4 mm $\times$ 11.4 mm, (b) 12.7 mm $\times$ 12.7 mm, and (c) 9.3 mm $\times$ 9.3 mm.

length is $\geqslant$0.5 mm while the membrane is 0.4 mm thick, so the pattern is quasi-two-dimensional. Each 8.3 mL volume reservoir is continuously refreshed at a flow rate of 20 mL per hour. The two reservoirs (delineated A and B) contain 0.8*M* sulfuric acid (A,B), 0.184*M* potassium bromate (A,B), 0.001*M* tris(2, 2′-bipyridyl)dichlororuthenium(II)hexahydrate (A), 0.22*M* malonic acid (B), and 0.2*M* sodium bromide (B). Under these conditions, the reaction is oscillatory and we observe rotating spiral waves of Ru(II) concentration in the membrane.

We image the spiral waves by passing spatially homogeneous low-intensity light through the membrane, and measure the relative intensity of the transmitted light using a CCD camera bandpass filtered at 451 nm. Regions of the glass membrane that contain Ru(II) absorb light at 451 nm; regions of high intensity have a lower concentration of Ru(II).

B. Resonant forcing

The ruthenium catalyst of the BZ chemical reaction is light-sensitive [23]. To periodically force the system, we apply time periodic spatially uniform pulses of light to the membrane. The particular effects of light using the same reactor setup we use here have been described previously [14].

We apply the parametric forcing using a commercial video projector (Sanyo PLC-750M) and a condensing lens. The video projector is computer controlled using a video card with a refresh rate of at least 0.1s. We temporally force the system, alternately projecting spatially homogeneous high-intensity and low-intensity light onto the membrane with a square wave time dependence.

C. Initial conditions

To test the predicted rate of curvature-driven coarsening, see Sec. III A, we measure the growth rate of circular patterns in the bistable 2:1 resonance regime. To create the initial pattern for this experiment, we project a radially symmetric pattern onto the membrane at a 1:1 resonance frequency. The chemical pattern responds with a radially symmetric pattern. After five forcing cycles, the circular chemical pattern is stable. We then spatially homogenize the light intensity and simultaneously change the forcing frequency so that it is in the 2:1 resonance regime. We create a 2:1 resonant pattern of concentric circles as shown in Fig. 2.

D. Data analysis

We determine the frequency of the chemical oscillations and show that the system is stably 2:1 locked using the pattern's temporal power spectrum. We calculate the power spectrum at each pixel in the image and average to determine the average power of the pattern. We consider the reaction 2:1 resonant with the forcing if the fundamental peak in the power spectrum is within one percent of half the forcing frequency.

The images shown in this paper were converted from snapshots of ruthenium concentration to a representation of the oscillation phases. This representation contains information for a complete oscillation cycle, i.e., it does not resolve the dynamics within a cycle. The chemical concentration oscillates exactly once for every two forcing cycles, resulting

FIG. 2. Example image of the chemical response to a radially symmetric forcing pattern. The pattern oscillates at half the forcing frequency (2:1 resonance). Black and white regions are oscillating π out of phase from each other. The image size is 7.6 mm $\times$ 7.6 mm. The chemical conditions are given in Sec. II A.

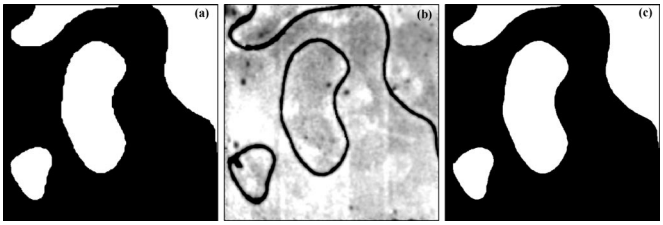

FIG. 3. Determination of domain boundaries for a 2:1 resonant pattern. (a) The phase and (b) the magnitude of each oscillation cycle were determined. (c) A combination of (a) and (b). The phase defines the interior of a domain and the magnitude defines the domain boundaries. The chemical conditions are given in Sec. II A. Image size: 11.4 mm×11.4 mm.

in two stable (π-shifted) oscillating states. Each pixel in an image is assigned to one of the two phase states. This removes information about the front width.

We use the magnitude of the oscillations to measure the front width. The front is the region where the local oscillation magnitude is changing, while magnitude is roughly uniform within a domain, see Fig. 3(b).

We match the location of the fronts from the magnitude data Fig. 3(b) with the domain boundaries from the phase data Fig. 3(a) to create the final images Fig. 3(c) shown in subsequent figures of this paper. Figure 3(c) is created by taking the pixel-by-pixel product of the phase and magnitude and applying a threshold to eliminate the variation of the magnitude in the interior of a domain. The final image has only phase information in the interior of the domains and magnitude information along the fronts. Thus, the width of a front is approximated from Fig. 3(b). The images we show in the following sections are obtained in the same way as Fig. 3(c).

III. DOMAIN COARSENING AND DOMAIN GROWTH

As we scan from low to high forcing frequency ω in the 2:1 resonance regime, we observe a transition from patterns coarsening, which includes both large domain and localized structure patterns, to growth of labyrinth patterns [9,10]. The transition occurs at a specific value ω_T. Coarsening patterns form below ω_T and labyrinth patterns form above ω_T in the 2:1 resonance regime.

As we scan back and forth in frequency, we measure that this transition does occur at a specific frequency, within the millihertz resolution of our experiments. However, the value of ω_T is sensitive to experimental parameters we cannot control, such as membrane age, therefore it is not meaningful for us to report a value for ω_T. On a given day, we observe a value of $\omega_T \pm 0.3$ mHz.

In the following subsections, we discuss the pattern selection in these different regimes.

A. Coarsening regime

Gomila *et al.* [20] examined the evolution of circular domains in numerical simulations of the FCGL amplitude equation. Simulations with forcing amplitudes above a critical value showed that a circular domain of one phase surrounded by π-shifted oscillations shrinks according to

$$R(t) = \sqrt{R(0)^2 - Dt}, \tag{2}$$

where R is the radius of a circular phase domain and D is the diffusion coefficient [20]. In the simulations, circular regions shrink when $D>0$ and grow when $D<0$; high curvature regions shrink more rapidly than low curvature ones according to Eq. (2).

In the 2:1 resonant regime below ω_T, we impose a radially symmetric initial condition in our experiments, see Sec. II C, and measure the radius R as a function of time. The sequence of snapshots in Fig. 4 shows an example of a circular domain shrinking. The minimum root-mean-square difference between a fit of $\log[R]$ versus $\log[R(0)^n - Dt]$ occurs for the fit when $n=2$ for circular patterns and the slope of the fit is 0.52 ± 0.04, demonstrating Eq. (2) is obeyed in the BZ system.

A quadratic fit of t versus R^2 for 23 measurements over a wide range of forcing strengths and forcing frequencies gives an average measure of the chemical diffusion coefficient. We obtain a value of $D = 2.2 \pm 0.2 \times 10^{-5}$ cm^2/s, which does not depend on the forcing parameters, and changes sign discontinuously at ω_T. This is in contrast to the FCGL results, where the value of D in Eq. (2) depends on the forcing parameters and goes smoothly through zero at the critical value. Additionally, this shrinking disk experiment provides a new technique to measure D in Vycor or other porous material, yielding a more precise value, which fits within previously reported estimates [24].

This curvature-driven front dynamics is also observed for arbitrarily shaped domains. Figure 5 shows that the local curvature $\kappa(t)$ changes according to Eq. (2) with $R(t) = 1/\kappa(t)$. The domains become locally more circular, and eventually vanish. The pattern in the last frame of Fig. 5 is still evolving. Asymptotically, it will be a single phase domain, or a pattern with stationary flat fronts separating phase domains.

To quantify the coarsening, we define the function $P(r,t)$ as the probability that two points a distance r apart are inside the same phase domain at time t. $P(r,t)$ is calculated using the following formula:

$$P(r,t) = \frac{1}{mn} \sum_i \sum_j \Theta(i,j;t)\,\delta(l_{ij} - r), \tag{3}$$

where i, j are pixel indices for an image, m is the total pixel number, n is the number of pixels a radius r away from i, $\Theta(i,j;t)=1$ for i, j in the same domain at time t, $\Theta(i,j;t) = 0$ for i, j in different domains, l_{ij} is the distance between the points indexed by i and j, and δ is the Dirac delta function. Therefore, $P(0,t)=1$.

The shape of the curve $P(r)$ for fixed t (see Fig. 6) captures the front roughness, i.e., how quickly $P(r)$ tends to zero depends on the probability that points are near the edge of a domain. This is more likely for domains with rough fronts. The average domain size is defined as the distance L such that $P(L,t)=1/2$. That is, pixels L away from an arbitrary pixel i have an equal probability of being inside or outside

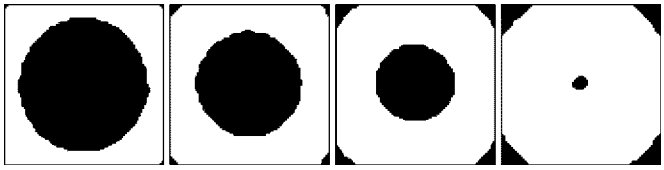

FIG. 4. Curvature-driven shrinking of a circular domain demonstrates the $t^{1/2}$ law, see text. Snapshots are evenly spaced in time at $t=0$, 821, 1641, and 2462 s. The domain vanishes at $t=2513$ s. Chemical conditions are the same as in Fig. 1. Image size is 3.2 mm $\times$ 3.2 mm.

the same domain as i. To capture the front roughness relative to the average domain size, L, we rescale r by L. Figure 6 shows $P(r,t)$ at various times for the data shown in Fig. 5. Rescaling r by the average domain size shows that the self-similar dynamics are independent of the pattern length scale. The inset of Fig. 6 shows that the average domain size depends linearly on $t^{1/2}$.

B. Localized structures

In our experiments, shrinking spots vanish for all forcing frequencies below ω_T in the bistable 2:1 resonant regime, except over a narrow range $\omega \lesssim \omega_T$, approximately $2-4$ mHz. In this regime, the asymptotic pattern is stable spots with radii of roughly 1 to 1.5 times the width of a front. The radius of these localized structures is approximately 0.34 ± 0.07 mm, while the width of a front is 0.26 ± 0.03 mm. Evolution of localized structures is shown in Fig. 7, and has been reported previously in [5,20]. While localized structures have been observed in the 2:1 resonance of the forced BZ system before [8], the fact that they are observed only in a narrow forcing frequency range and that they form via the coarsening mechanism has yet to be reported.

Localized structures have been reported for parameter values near the transition to labyrinths in amplitude equations [20,25], which have shown that the tails of the fronts have a repulsive interaction that acts against the curvature-driven mechanism at short range. This is consistent with our observation that the shrinking of domains stops when the fronts come close to each other.

Other stable patterns in this regime include a target pattern, where a localized structure exists at the center, surrounded by a ring with a width equal to the localized structure diameter. A similar pattern might have two or more localized structures at the center.

C. Labyrinths

When ω is tuned above ω_T, we observe a transition from domain coarsening to domain growth and tip splitting in regions of high curvature. The snapshots in Fig. 8 show the time evolution of a labyrinth pattern. We are unable to measure the growth rate of these domains, due to the transverse instability of fronts in this regime [10]. In experiments reported here, measurement is also hindered by breakup of the uniform oscillations (nucleation mechanism) [10] within a domain. This instability of spatially uniform oscillations can

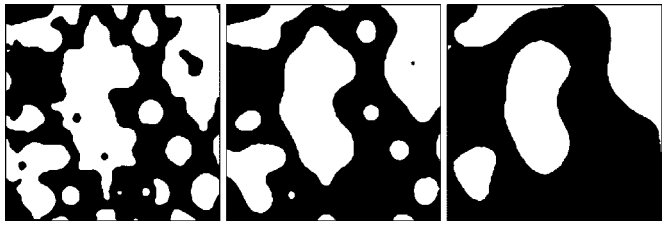

FIG. 5. The time evolution of a pattern coarsening at $\omega = 0.039$ Hz. $t=0$, 461, and 1640 s. High curvature fronts coarsen more rapidly. As a domain becomes smaller, the curvature increases and eventually the domain vanishes. The asymptotic pattern will contain either a single phase or flat fronts, and will take several hours to reach. Chemical conditions given in Sec II A. Image size is 11.4 mm $\times$ 11.4 mm.

be seen in the first frame of Fig. 8. Although we cannot measure the rate, we do observe that domains grow in this parameter regime. Our experimental observations are in agreement with numerical studies of the FCGL equation, where curvature-driven growth [20] was found for $D<0$ in Eq. (2) when ω is above ω_T.

The front interaction which stabilizes localized structures also stabilizes the labyrinth patterns. In experiments, the labyrinth tips repel each other when they get close. This growth-limiting mechanism sets a characteristic wavelength, approximately 0.67 mm in our experiments. This is also the diameter of the observed localized structures.

IV. DISCUSSION

To gain insight into the underlying physics of the coarsening mechanism in the periodically forced BZ system, we consider two descriptions. The first description is purely geometric, requiring only that the area covered by each half of a front breathing cycle is proportional to the length of the front. The second description is from a kinematic point of view, using Eq. (1).

The chemical kinetics of the BZ system is strongly excitable in the parameter regime in which we conduct experiments. Thus, in the absence of perturbations, the system would be in a stable, time-independent state. However, the strong excitability of the kinetics in conjunction with the spatial extent of the real system (which contains sources of noise, e.g., from boundaries) results in continuous self-sustained relaxation oscillations. Thus, the system we study is both oscillatory, in the sense that it is autonomously time-periodic, and excitable, in the sense that part of the periodic cycle is in a true refractory period, during which perturbations decay exponentially.

The geometric argument we pose first invokes both the oscillatory and diffusive nature of the bistable system, as well as the excitable nature of the chemical reaction. First, we discuss the features of excitability relevant to curvature-driven front dynamics, then we discuss the interplay of the excitability, diffusion, oscillations, and geometry.

An excitable process (chemical reaction) is the interplay of two agents, an activator and an inhibitor. Examples of excitable behavior include action potentials in nerve cells,

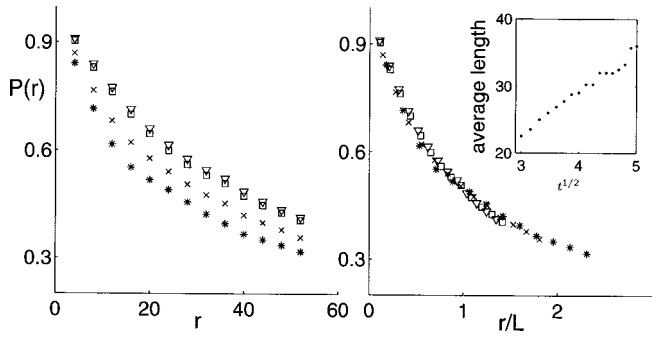

FIG. 6. Left: The probability function $P(r,t)$ for times $t=0$, 308, 974, and 1282 s (*, ×, □, and ∇, respectively). Right: Scaling each probability function by the average domain size L demonstrates that the dynamics are independent of length scale.

the beating of the heart, combustion processes, and the BZ chemical reaction. In the BZ reaction, the activator bromous acid enhances its own production. This autocatalytic process causes a rapid increase in activator concentration. The excitation process is inhibited by free bromide ion concentration [24].

To describe the fast oscillations of the front dynamics, we treat diffusion and reaction independently. In particular, we consider the direction of diffusion but not the magnitude. Figure 9 shows, for the special case of a 2D flat front, the activator species diffusing from high to low concentration, which occurs over a time interval t_0 to t_1. Frame t_2 shows the start of the second half of the cycle. Temporal oscillations of the activator and inhibitor concentrations cause a reversal of the location of excited and nonexcited domains. Note, the position of the front (solid line) remains the same from t_1 to t_2 since we are considering the diffusion and reaction separately. The diffusion then occurs in the opposite direction and, as indicated by the dashed line, the front returns to its original location. The cycle is complete when the reaction oscillation returns the activator concentration to the original levels shown in frame t_0. The flat front of the activator species diffuses into the unexcited region traveling a distance Δx and covering an area equal to the length of the front times Δx. In contrast, a curved 2D front will not return to the same position, as we will describe next.

In the coarsening regime, during one cycle of the pattern oscillation a circular domain expands and then contracts. The

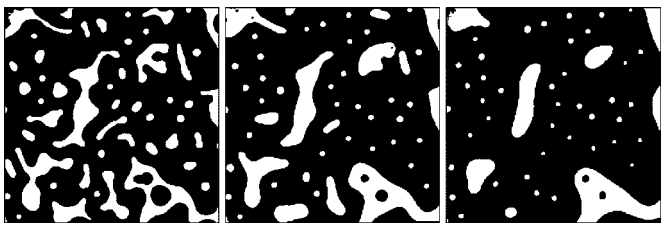

FIG. 7. Snapshots show the time evolution of a pattern as it coarsens to localized structures. $t=0$, 379, and 1344 s. The small circular domains in the last frame are stable. Their radius is 0.34 ± 0.07 mm. The domains in these images larger than the localized structure size continue to shrink. Chemical conditions are given in Sec II A. Image size is 12.7 mm × 12.7 mm.

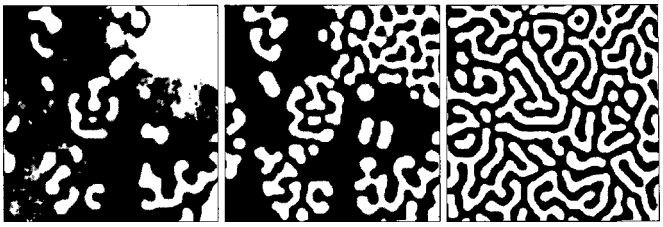

FIG. 8. Time evolution of a labyrinth pattern, $t=0$, 290, and 1032 s. The growth of a labyrinth occurs along fronts with high curvature. The labyrinth pattern in the final frame does not change qualitatively in time. Chemical conditions are given in Sec. II A. Image size is 9.3 mm × 9.3 mm.

change in area of a circle expanding or contracting is simply the circumference times Δx. During expansion, the total increase in area is $\Delta A=2\pi r_0\Delta x$, where r_0 is the initial radius, before expansion. The radius after expansion is

$$r_{1/2}=\sqrt{\frac{A_0+\Delta A}{\pi}}=\sqrt{r_0^2+2r_0\Delta x}, \tag{4}$$

where $r_{1/2}$ is the radius of the circle after one half oscillation. Note that $r_{1/2}$ is less than $r_0+\Delta x$. This geometric picture indicates that the change in the radius during expansion is less than Δx.

During the second half of the oscillation, the front contracts. The decrease in area of the circle is now $2\pi r_{1/2}\Delta x$ and the radius after one full cycle, r_1, is

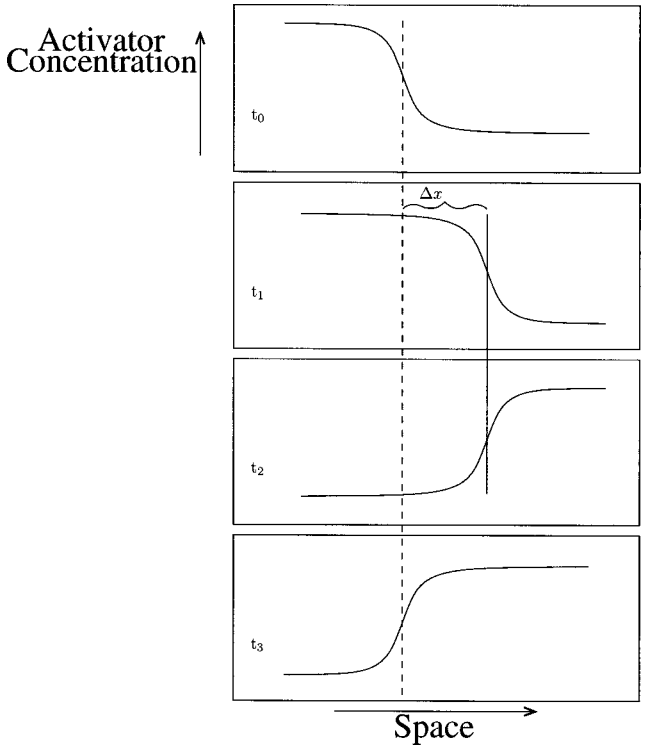

FIG. 9. In one breathing cycle, a 1D front returns to its original position after traveling a distance Δx in each direction.

$$r_1 = \sqrt{r_0^2 + 2r_0\Delta x - 2\Delta x\sqrt{r_0^2 + 2r_0\Delta x}}. \quad (5)$$

Thus during contraction, the radius changes by an amount more than Δx, i.e., more than it grew during expansion. Hence, over one cycle the total domain size shrinks.

Additionally, we derive the relationship between Δx and the parameter D from Sec. III A, which shows that the short time scale breathing, Δx, drives the longer time scale coarsening. The change in the radius for a given cycle, $\Delta r = r_1 - r_0$, is

$$\Delta r = \sqrt{r_0^2 + 2r_0\Delta x - 2\Delta x\sqrt{r_0^2 + 2r_0\Delta x}} - r_0. \quad (6)$$

If $r_0 >> \Delta x$, then expanding the square roots yields $\Delta r = -\Delta x^2/r$ is the change in r during one oscillation. To consider the period averaged behavior, we divide each side by the period of oscillation and consider the left-hand side to be differentials instead of finite differences,

$$\frac{dr}{dt} = \frac{\Delta x^2}{rT}, \quad (7)$$

where T is the period of oscillation. When we integrate this equation, we recover $R = \sqrt{R(0)^2 - Dt}$ with $D = 2\Delta x^2/T$.

Depending on the duration of the refractory part of the cycle, the breathing of a curved front can cause a circular domain to either shrink or grow (Secs. III A and III C). When the observed refractory time is short, shrinking occurs. The diffusion of the activator excites the nonexcited state, which causes the excited domain to expand. In contrast, when the refractory time is longer, the activator diffuses into the nonexcited region without causing excitation. Consequently, r_1 is greater than Δx after one cycle and domains grow.

A kinematic approach [Eq. (1)] captures the breathing motion of fronts as an excitation wave moving into an unexcited region. Oscillations in the excited (white) domains become unexcited (black) after half a pattern cycle, causing the front velocity to switch direction. For a curved front, κ is positive when domains expand and negative when domains contract.

The two stages of breathing are

$$V = \frac{dr}{dt} = V_0 \pm \frac{1}{r}D. \quad (8)$$

Solving Eq. (8) shows that the change in r while contracting is greater than the change in r while expanding by the amount $2D\tau/r_0$, where τ is the amount of time for each expansion and contraction. For a single cycle, expansion and contraction occur for one-quarter of the oscillation period each. This is because the domain is expanding for 1/2 the cycle and contracting for the other 1/2, except when the forcing light, which acts as an inhibitor, is on. Thus, $\tau = T/4$, and Δr, the total change in radius over one cycle of the pattern, is $\Delta r = -DT/2r$.

From this relation comes

$$\frac{dr}{dt} = \frac{-D}{2r}, \quad (9)$$

which is equivalent to Eq. (7) when $D = 2\Delta x^2/T$. Thus, these two descriptions are consistent with both the experimental data and each other.

ACKNOWLEDGMENTS

We thank Linda Smolka for useful discussions, and we acknowledge support from Oak Ridge Associated Universities and NSF Grant DMR-0348910.

[1] L. Leibler, Macromolecules **13**, 1602 (1980).
[2] R. Sessoli, D. Gatteschi, A. Caneschi, and M. A. Novack, Nature (London) **365**, 141 (1993).
[3] R. Bascones, J. Garcia-Ojalvo, and J. M. Sancho, Phys. Rev. E **65**, 061108 (2002).
[4] M. Meixner, P. Rodin, E. Scholl, and A. Wacker, Eur. Phys. J. B **13**, 157 (2000).
[5] V.B. Taranenko, K. Staliunas, and C. O. Weiss, Phys. Rev. Lett. **81**, 2236 (1998).
[6] V. K. Vanag, L. Yang, M. Dolnik, A. M. Zhabotinsky, and I. R. Epstein, Nature (London) **406**, 389 (2000).
[7] A. Hagberg and E. Meron, Phys. Rev. Lett. **78**, 1166 (1997).
[8] V. Petrov, Q. Ouyang, and H. L. Swinney, Nature (London) **388**, 655 (1997).
[9] A. L. Lin, M. Bertram, K. Martinez, H. L. Swinney, A. Ardelea, and G. F. Carey, Phys. Rev. Lett. **84**, 4240 (2000).
[10] A. Yochelis, A. Hagberg, E. Meron, A. L. Lin, and H. L. Swinney, SIAM J. Appl. Dyn. Syst. **1**, 236 (2002).
[11] A. L. Lin, A. Hagberg, A. Ardelea, M. Bertram, H. L. Swinney, and E. Meron, Phys. Rev. E **62**, 3790 (2000).
[12] M. Markus, G. Kloss, and I. Kusch, Nature (London) **371**, 402 (1994).
[13] V. K. Vanag, A. M. Zhabotinsky, and I. R. Epstein, Phys. Rev. Lett. **86**, 552 (2001).
[14] K. Martinez, A. L. Lin, R. Kharrazian, X. Sailer, and H. L. Swinney, Physica D **168**, 1 (2002).
[15] P. Foerster, S. Muller, and B. Hess, Science **241**, 685 (1988).
[16] P. Brazhnik *et al.*, Chaos, Solitons Fractals **10**, 99 (1999).
[17] J. J. Tyson and J. P. Keener, Physica D **32**, 327 (1988).
[18] P. K. Brazhnik and J. J. Tyson, Phys. Rev. E **59**, 3920 (1999).
[19] A. S.Mikhailov and V. S. Zykov, Physica D **52**, 379 (1991).
[20] D. Gomila, P. Colet, G.-L. Oppo, and M. San Miguel, Phys. Rev. Lett. **87**, 194101 (2001).
[21] B. Marts, A. Hagberg, E. Meron, and A. L. Lin, Phys. Rev. Lett. **93**, 108305 (2004).
[22] R. Gallego, M. San Miguel, and R. Toral, Phys. Rev. E **61**, 2241 (2000).
[23] S. Kadar, T. Amemiya, and K. Showalter, J. Phys. Chem. A **101**, 8200 (1997).
[24] A. Belmonte, Q. Ouyang, and J.-M. Flesselles, J. Phys. II **7**, 1425 (1997).
[25] V. J. Sanchez-Morcillo and K. Staliunas, Phys. Rev. E **60**, 6153 (1999).